ANALYSIS OF THE DCB TEST OF ANGLE-PLY LAMINATES INCLUDING RESIDUAL STRESSES

J. De Gracia[a,*], A. Boyano[a], A. Arrese[b], F. Mujika[b]

Materials+Technologies/Mechanics of Materials Group

[a] Department of Mechanical Engineering, Faculty of Engineering of Vitoria-Gasteiz, University of the Basque Country (UPV/EHU), Nieves Cano, 12, 01006 Vitoria-Gasteiz, Spain

[b] Department of Mechanical Engineering, Faculty of Engineering of Gipuzkoa, University of the Basque Country (UPV/EHU), Plaza de Europa, 1, 20018 San Sebastián, Spain

*Corresponding author. E-mail: juan.degracia@ehu.es

Abstract

A new method for obtaining energy release rate by the Double Cantilever Beam test for angle-ply laminates is proposed. Two different sequences, symmetric and anti-symmetric, have been studied. The fact that the layers are oriented at different angles and the residual stresses, causes the existence of mixed mode fracture. The analytical model presented, based on the complementary energy of a laminated beam, is an extension of a previous model for unidirectional laminates and includes hygrothermal effects. Experimental results of the energy release rate obtained by means of the area method agree with those determined by the proposed approach.

Keywords; Delamination; Double Cantilever Beam; Multidirectional.

1. Introduction

Delamination is one of the most common failures in laminated composites due mainly to the low interlaminar strength of these materials. The double cantilever beam (DCB)

test is widely used to measure mode I critical Energy Release Rate G_{Ic} of unidirectional laminates and has been standardized for carbon fiber reinforced plastic (CFRP) specimens [1, 2].

The standards describe three reduction methods that lead to calculate G_{Ic}: the modified beam theory, the compliance calibration method and the modified compliance calibration method. Results from different methods do not differ more than 3.1% [3]. In spite of standards have been developed for unidirectional specimens, these methods have been often used to calculate G_{Ic} of multidirectional laminates [4, 5, 6]. Nevertheless, some factors which are less effective in unidirectional DCB specimens may affect seriously in the case of multidirectional specimens [7], such as laminate lay-up, symmetry of the laminate, curved crack front, mode mixture, residual stresses or damage during the crack growth (fiber bridging effect, fiber matrix debonding, or fiber breakage). Nicholls et al. [8] investigated the critical value of G in multidirectional CFRPs reporting that the crack can move to other interfaces. They identified four different crack morphologies. The stacking sequence in multidirectional specimens is related to crack front shape since bending-bending and bending-twisting couplings contribute to curved and un-symmetric crack fronts respectively [9, 10, 11]. An appropriate selection of the stacking sequence may prevent those issues, making their effect on G_{Ic} negligible and leading to a nearly pure mode I [12].

Taking all these factors into account, in addition to the fact that initiation value is the most conservative toughness value, delamination toughness from the DCB test on multidirectional laminates should probably be quantified just for initiation values. Some studies have come to the conclusion that the initiation value for G_{Ic} is practically independent from the ply orientation of the delaminating interface [6, 13], while others

state the opposite [14, 15].

Extensive research concerning this field has been led to develop analytical solutions for DCB unidirectional specimens as well as multidirectional ones. Kanninen [16] modeled, for isotropic materials, each arm of the DCB specimen as a beam on an elastic foundation. Williams [17] completed Kanninen's model for orthotropic materials, while Ozdil and Carlsson [18] extended it to angle-ply laminates. Olsson [19] determined the end displacement caused by the transverse compliance in the un-cracked part and the Saint Venant effects ahead the crack front. Szekrényes [20] presented an improved analysis including Winkler–Pasternak foundation, transverse shear, Saint–Venant effect and crack tip shear deformation. Shokrieh et al. [21] revised solutions that model each arm of the specimen as a beam on an elastic foundation. Weatherby [22] included a rotational spring to a clamped beam in order to incorporate the rotation at the crack tip. This model has been later used by other authors [23, 24]. In the last years computer based methods such as the virtual crack closure technique and the cohesive zone model have been widely used [25, 26, 27]. The previous studies regarding interlaminar toughness in multidirectional laminates are in general applied to stacking sequences that avoid bending-twisting coupling, due to the difficulties related to twisting curvatures associated to mode III. These models, generally, do not deal with the residual stress due to hygrothermal effects. Nairn [28] studied the energy release rate for adhesive and laminate DCB specimens with consideration of the effect of residual stress concluding that the errors are large when the delaminating arms are un-symmetric laminates and these effects are not taken into account.

Concerning unidirectional laminates a new model for determining G_I has been recently proposed [29]. Besides the determination of new compliance and energy release rate equations, the analytical model presented leads to calculate the crack length for every

pair of load and displacement values, without any optical measurement. Therefore, a continuous plot of the R-curve of the specimen is obtained, allowing the study of the behavior of the laminate during the propagation period.

The aim of the present study is to estimate G for carbon/epoxy angle-ply symmetric and anti-symmetric laminates by means of the DCB test. With this purpose, a new analytic approach based on the complementary energy of a laminated beam including hygrothermal effects is used for the first time, to the best of our knowledge. In that way, the model presented in [29], for calculating G_{Ic} in unidirectional laminates, is extended to angle-ply laminates.

Two different sequences will be studied in this paper: $\left[\left(\pm 45\right)_4\right]_{as}$ anti-symmetric and $\left[\left(\pm 45\right)_4\right]_s$ symmetric laminates. These sequences have been chosen due to the fact that they have different fiber orientation of the adjacent plies in the mid-plane although both have equal properties for each one of the sub-laminates separated by the delaminating interface. Moreover, hygrothermal effects are also different in both cases.

Nomenclature

a	Effective crack length (mm)
$[a],[b],[c]$	Compliance matrices
a_{mn}	In-plane compliance coefficients (mm/N)
b	DCB specimen width (mm)
b_{mn}	Coupling compliance coefficients (N)
d_{mn}	Flexural compliance coefficients (1/N-mm)
$\{e\}_k$	Hygrothermal strains matrix at lamina k

F_1, F_2, F_3 Equivalent point forces for distributed load (N)

G_I, G_{II}, G_{III} Strain energy release rate in mode I, II, III (J/m^2)

G_C Critical strain energy release rate (J/m^2)

L Length of the specimen (mm)

$\{\bar{M}\}$ Matrix of the sum of mechanical and hygrothermal moments

M_i Bending moment per unit length at section i (N)

M_{s_i} Twisting moment per unit length at section i (N)

M_s^{HT} Hygrothermal twisting moment per unit length (N)

m_i Bending moment at section i (N-mm)

m_{t_i} Twisting moment at section i (N-mm)

$\{\bar{N}\}$ Matrix of the sum of mechanical and hygrothermal forces

N_x^{HT}, N_y^{HT} Hygrothermal forces per unit length (N/mm)

P Opening load on the DCB specimen (N)

$[Q]_k$ Reduced stiffness matrix at lamina k

q_{10}, q_{30} Maximum intensities of the distributed forces in the model (N/m)

U^* Complementary strain energy (N/m)

x_1, x_2, x_3 Parameters of the distributed forces model (mm)

z_k Distance from the mid-plane to the lower surface of the k^{th} layer.

α_0, α_1 Parameters depending on x_1, x_2, x_3

δ_i Generalized displacement at point i in the direction of the generalized force F_i

κ_s^{HT} Twisting curvature due to hygrothermal twisting moment

2. Anti-symmetric laminates.

2.1. Load-strain relations.

In this study $\left[\left(\pm 45\right)_4\right]_{as}$ anti-symmetric and $\left[\left(\pm 45\right)_4\right]_{s}$ symmetric laminates have been considered. In both cases the sub-laminates, that is, the crack arms of the delaminated region are anti-symmetric.

An anti-symmetric laminate has its plies of the same thickness and material above and below the mid-plane but they and are oriented at $+\theta$ and $-\theta$. In addition, in the event that plies have a single value of θ they are called regular anti-symmetric angle-ply laminates.

The constitutive relation for an anti-symmetric regular laminate is given by [30].

$$\left\{\begin{array}{c} \varepsilon_x^0 \\ \varepsilon_y^0 \\ \gamma_s^0 \\ \hdashline \kappa_x \\ \kappa_y \\ \kappa_s \end{array}\right\} = \left[\begin{array}{ccc:ccc} a_{xx} & a_{xy} & 0 & 0 & 0 & b_{xs} \\ a_{yx} & a_{yy} & 0 & 0 & 0 & b_{ys} \\ 0 & 0 & a_{ss} & b_{sx} & b_{sy} & 0 \\ \hdashline 0 & 0 & b_{xs} & d_{xx} & d_{xy} & 0 \\ 0 & 0 & b_{ys} & d_{yx} & d_{yy} & 0 \\ b_{xs} & b_{sy} & 0 & 0 & 0 & d_{ss} \end{array}\right] \left(\left\{\begin{array}{c} N_x \\ N_y \\ N_s \\ \hdashline M_x \\ M_y \\ M_s \end{array}\right\} + \left\{\begin{array}{c} N_x^{HT} \\ N_y^{HT} \\ 0 \\ \hdashline 0 \\ 0 \\ M_s^{HT} \end{array}\right\} \right) \tag{1}$$

The fact that bending-twisting coupling is not present in the stacking sequences studied, leads to the possibility of analyzing bending and twisting separately. In addition, as the angle selected in this work is 45º it results in these relations between compliance coefficients:

$$a_{xx} = a_{yy}; \quad d_{xx} = d_{yy}; \quad b_{xs} = b_{ys} \tag{2}$$

Regarding hygrothermal effects, although material operates at room temperature, equivalent hygrothermal loads due to cooling down from processing temperatures should be taken into account. In the sequences studied herein, the non-zero

hygrothermal loads are N_x^{HT} and N_y^{HT} forces and M_s^{HT} twisting moment. Besides, $N_x^{HT} = N_y^{HT}$ due to $\theta = 45^{\circ}$.

2.2. Complementary strain energy and its derivatives

The complementary strain energy in a multidirectional laminate due to in-plane stresses can be expressed as follows [31]:

$$U^* = \frac{1}{2}\int_{L_x}\int_{L_y}\left(\{\bar{N}\}^t[a]\{\bar{N}\} + 2\{\bar{N}\}^t[b]\{\bar{M}\} + \{\bar{M}\}^t[d]\{\bar{M}\}\right)dxdy \\ -\frac{Lb}{2}\sum_{k=1}^{n}\{e\}_k^t[Q]_k\{e\}_k\left(z_k - z_{k-1}\right) \tag{3}$$

Where z_k denotes the distance from the mid-plane to the lower surface of the k^{th} layer. L_x and L_y indicate length and width direction respectively. L is the total length of the specimen; $\{\bar{N}\}$ is the matrix of the sum of mechanical and hygrothermal forces and $\{\bar{M}\}$ is the matrix of the sum of mechanical and hygrothermal moments.

A system in equilibrium subjected to independent F_i generalized forces and a crack of length a is considered. By applying the first principle of Thermodynamics in terms of the complementary energy and assuming that an infinitesimal crack advance is a reversible process, and consequently the complementary energy is an exact differential, the following results are obtained [32]:

$$\delta_i = \left(\frac{\partial U^*}{\partial F_i}\right)_a \tag{4}$$

$$G = \frac{1}{b}\left(\frac{\partial U^*}{\partial a}\right)_{F_i} \tag{5}$$

Eq. (4) is the Engesser-Castigliano's theorem, being δ_i the generalized displacement in

the direction of F_i. Eq. (5) gives the energy release rate G, being b the crack width.

Differentiating (3) with respect to F_i and a, taking into account that hygrothermal terms do not depend on those variables, Eqs. (4) and (5) become in:

$$\delta_i = U^*_{,F_i} = b\int_{L_x} \begin{pmatrix} \{N\}^t_{,F_i}[a]\{\bar{N}\} + \{N\}^t_{,F_i}[b]\{\bar{M}\} \\ +\{M\}^t_{,F_i}[b]\{\bar{N}\} + \{M\}^t_{,F_i}[d]\{\bar{M}\} \end{pmatrix} dx \tag{6}$$

$$G = U^*_{,a} = \frac{\partial}{\partial a}\left[\frac{1}{2}\int_{L_x}\left(\{\bar{N}\}^t[a]\{\bar{N}\} + 2\{\bar{N}\}^t[b]\{\bar{M}\} + \{\bar{M}\}^t[d]\{\bar{M}\}\right)dx\right] \tag{7}$$

As in Eq.(7) the integral limits depend on the crack length, Leibniz`s integral rule can be applied in order to obtain the derivative with respect to a. It states that given a function $f = f(x,a)$,

$$\frac{\partial}{\partial a}\left(\int_{a(a)}^{b(a)} f(x,a)\,dx\right) = \int_{a(a)}^{b(a)} \frac{\partial f(x,a)}{\partial a}dx + f\left(b(a),a\right)b`(a) - f\left(a(a),a\right)a`(a) \tag{8}$$

3. Analytical approach

3.1. Applied and redundant loads

3.1.1. Bending moment

With the aim to calculate the distribution of bending moments the approach presented by De Gracia et al. [29] has been followed. This method, besides the determination of compliance and energy release rate equations, leads to calculate the crack length for every pair of load and displacement values without any optical measurement. The method takes into account large displacements and local deformation effects.

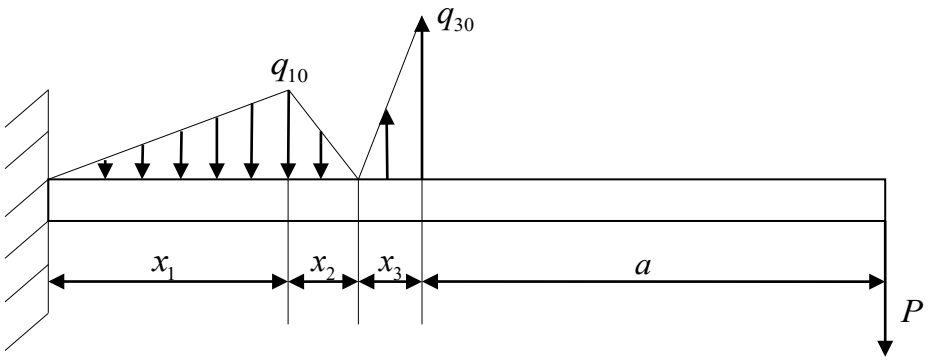

Fig. 1 Distributed force along the beam.

Fig. 1 shows a simplified model of the distributed forces ahead of the crack tip for the upper half of the DCB specimen, where a is the effective crack length, P the applied load, x_1, x_2, x_3 are the lengths of the bases of the distributed loads, while q_{10} and q_{30} are their maximum intensities, located at sections 1 and 3 respectively. It is assumed that distributed loads equilibrate the effect of the applied load. Thus, force and moment at the clamped end are null. In addition, taking into account that the studied specimens have not a straight delamination front, a is defined as an effective length.

Displacements at sections 1, 2 and 3 are determined by the Engesser-Castigliano's theorem and equated to those obtained by imposing that the displacements at the sections correspond to the transverse deformation in the specimen. Applying also static equilibrium the values of x_1, x_2, x_3, q_{10} and q_{30} are obtained as a function of the mechanical properties of the material, the geometry of the specimen, and the applied load P. With respect to x_3, although it depends on the crack length, its variation with the usual values of a is not meaningful and can be considered constant.

Once the parameters of the model have been determined, the distributions of bending moments m_x corresponding to the whole section are determined as a function of the crack length a, being:

$$\begin{cases} m_{x_1} = -F_1 \dfrac{x^3}{3x_1^2} \\ m_{x_2} = \dfrac{F_1}{3x_2x_1}\left(x^3 - \left(3x_1 + 3x_2\right)x^2 + \left(3{x_1}^2 + 3x_2x_1\right)x - {x_1}^3 - x_2{x_1}^2\right) \\ m_{x_3} = -F_1\left(\dfrac{x_2 + x_1}{x_1}x + \dfrac{-{x_2}^2 - 3x_2x_1 - 2{x_1}^2}{3x_1}\right) + F_3\dfrac{\left(x - x_1 - x_2\right)^3}{3{x_3}^2} \\ m_{x_a} = -F_1\left(\dfrac{x_2 + x_1}{x_1}x + \dfrac{-{x_2}^2 - 3x_2x_1 - 2{x_1}^2}{3x_1}\right) + F_3\left(x - x_1 - x_2 - \dfrac{2x_3}{3}\right) \end{cases} \quad (9)$$

Where $F_1 = \dfrac{q_{10}x_1}{2}$; $F_3 = \dfrac{q_{30}x_3}{2}$.

3.1.2. Twisting moment

Residual stresses induce a rotation in each cracked arm. While in the case of anti-symmetric laminates both arms rotate in the same sense (Fig. 2b), in the case of symmetric laminates there are opposing rotations (Fig. 2a) related to mode III of fracture. Then, assuming that the twisting rotation at the load application is prevented in the case of symmetric laminates, a twisting moment should be applied by the piano hinges. Actually, there is a non-uniform load distribution applied on the piano hinges, whose resultant is the applied force P and the resultant moment is the twisting moment.

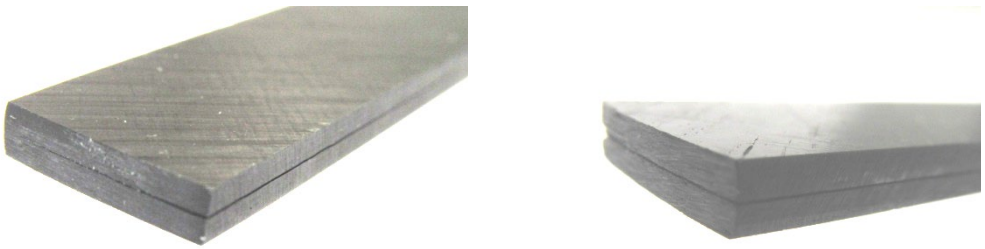

Fig. 2 Deformation due to the hygrothermal moments. a) Symmetric laminate. b) Anti-symmetric laminate.

Fig. 3 shows the twisting moment at the load application point and the reactive twisting moment applied at the crack front, related to the non uniform distribution along the width of the distributed forces shown in Fig. 1. It is assumed that this moment is concentrated at the crack front. Those moments are equal and opposite.

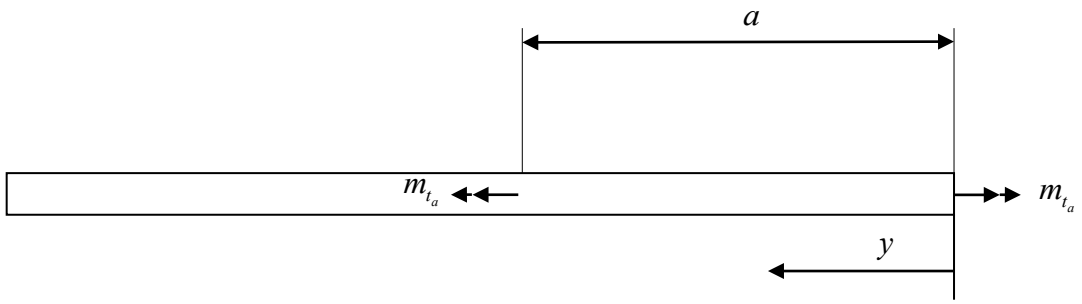

Fig. 3 Twisting moment.

Thus, force and moment resultants are given by:

$$\left\{\bar{N}\right\} = \begin{Bmatrix} N_x^{HT} \\ N_y^{HT} \\ 0 \end{Bmatrix} \tag{10}$$

$$\left\{\bar{M}\right\} = \begin{Bmatrix} M_x \\ 0 \\ M_s + M_s^{HT} \end{Bmatrix} \tag{11}$$

As a first approach, it is assumed that the distribution of M_s is uniform along the width. The theorem of Engesser-Castigliano will be used in order to calculate the twisting moment applied by the piano hinges. Since piano hinges prevent rotation at the load application point, the derivative of the complementary energy with respect to the twisting moment applied at the load point is zero. Replacing Equations (10) and (11) in Equation (6) and taking into account the properties of anti-symmetric laminates described in section 2.1, it gives:

$$U^{*}_{,X} = \frac{1}{2}\int_{L_x}\int_{L_y}\left(\left(4b_{xs}N_x^{HT} + 2d_{ss}M_s^{HT}\right)M_{s,X} + 2d_{ss}M_s M_{s,X}\right)dxdy = 0 \tag{12}$$

Where $X = m_{t_a}$

The half of the whole twisting moment m_t of a rectangular section corresponds to M_s and the other half correspond to the resultant moment of out-of-plane shear forces [33]:

$$\begin{aligned} \tfrac{1}{2}m_t &= \int_b M_s dy \\ \tfrac{1}{2}m_t &= \int_b V_r y dy \end{aligned} \tag{13}$$

The distribution of twisting moments is:

$$m_t = m_{ta} \quad 0 < y < a \tag{14}$$

Replacing distribution given in Eq. (14) after taking into account Eq. (13), the redundant unknown is:

$$m_{t_a} = -2b\left(\frac{2b_{xs}}{d_{ss}}N_x^{HT} + M_s^{HT}\right) \tag{15}$$

According to Eq. (15) m_{t_a} does not depend on the crack length.

3.1.3. Shear force

In the case of an anti-symmetric DCB specimen (Fig. 2a), hygrothermal twisting moment generates rotations of the same sense in both cracked arms. Then, the specimen remains horizontal at the load application, and consequently the non-cracked part and the crack front have a twisting rotation, as shown in Fig. 4. As a consequence, there are opposite in plane N_s forces in each cracked arm at the crack tip, related to mode III fracture.

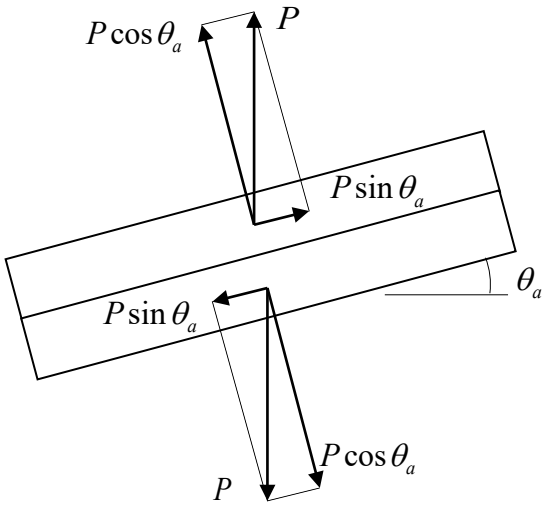

Fig. 4 P force and its components at the crack tip

Force and moment resultants for this case are:

$$\left\{\overline{N}\right\} = \begin{Bmatrix} N_x^{HT} \\ N_y^{HT} \\ N_s \end{Bmatrix} \tag{16}$$

$$\left\{\overline{M}\right\} = \begin{Bmatrix} M_x \\ 0 \\ M_s^{HT} \end{Bmatrix} \tag{17}$$

The angle θ_a rotated by the laminate at the crack front can be obtained through [34]:

$$\theta_a = \frac{\kappa_s^{HT}}{2} a \tag{18}$$

Where κ_s^{HT} is the twisting curvature of the laminate due to hygrothermal twisting moment. Assuming that the angle θ_a is very small, $\sin\theta_a \approx \theta_a$ and thus the distribution of the shear force per unit length can be expressed as:

$$N_s = \frac{\kappa_s^{HT} P}{2b} y \quad 0 < y < a \tag{19}$$

3.2. Energy Release Rate

3.2.1. Symmetric laminate $\left[\left(\pm 45\right)_4\right]_s$

With the objective of obtaining an expression of the complementary energy as a function of the crack length, the expressions for bending moments and twisting moments obtained in Eqs. (9) and (15) are replaced in (7).

It is worth noting that terms in Eq.(7) not affected by applied loads are integrated along all the length L, and do not depend on the crack length a. Therefore, the derivative of these terms with respect to a is null.

Taking into account all the above mentioned:

$$G = \frac{d_{xx} P^2}{b^2}\left(\alpha_0 + \alpha_1 a + a^2\right) - d_{ss}\left(\frac{2b_{xs}}{d_{ss}} N_x^{HT} + M_s^{HT}\right)^2 \tag{20}$$

Where factors α_0 and α_1 just depend on the dimensions x_1, x_2 and x_3.

Terms affected by d_{xx} in Eq. (20) can be considered the part of the energy release rate due to fracture mode I and the second term corresponds to fracture mode III. Therefore the contribution of modes I and III are:

$$G_I = \frac{P^2 d_{xx}}{b^2}\left(\alpha_0 + \alpha_1 a + a^2\right) \tag{21}$$

$$G_{III} = -d_{ss}\left(\frac{2b_{xs}}{d_{ss}} N_x^{HT} + M_s^{HT}\right)^2 \tag{22}$$

The physical meaning of the negative sign of G_{III} is related to the fact that hygrothermal effects induce an initial mode III deformation without any load, as can be seen in Fig. 2a. Therefore, when the load is applied, the total energy necessary for the crack advance is less, although the total amount is positive.

3.2.2. Anti-symmetric laminate $\left[(\pm 45)_4\right]_{as}$

A similar process to the one used in the previous section, leads to the expression for determining the energy release rate G for anti-symmetric laminates. Replacing bending moments and forces obtained in (9) and (19) in Eq.(7):

$$G = \frac{d_{xx}P^2}{b^2}\left(\alpha_0 + \alpha_1 a + a^2\right) + \frac{\kappa_s^{HT} P^2 a^2}{b^2}\left(\frac{a_{ss}\kappa_s^{HT}}{4} + b_{xs}\right) \tag{23}$$

As it has been explained for symmetric laminates, terms affected by d_{xx} are related to mode I while the other term corresponds to fracture mode III:

$$G_I = \frac{d_{xx}P^2}{b^2}\left(\alpha_0 + \alpha_1 a + a^2\right) \tag{24}$$

$$G_{III} = \frac{\kappa_s^{HT} P^2 a^2}{b^2}\left(\frac{a_{ss}\kappa_s^{HT}}{4} + b_{xs}\right) \tag{25}$$

It is worth noting, as can be seen by comparing Eq.(20) and (23), that the part of the energy release rate corresponding to fracture mode I is the same in both configurations studied, while the energy due to mode III differs, depending on the crack length in the case of an anti-symmetric laminates. As in the previous case, G_{III} is negative since in the sequence studied b_{xs} is negative and predominant over the other term.

4. Experimental

The material used in this study is T6T/F593, a thermosetting epoxy resin (F593) reinforced by Toray T300 continuous carbon fiber provided by Hexcel Composites. Elementary plies of unidirectional material with a 55% volume-content of fiber were used to manufacture angle-ply laminates by hot press molding. The mechanical and thermal characteristics of unidirectional prepregs are summarized in **Table 1**.

$E_x(GPa)$	$E_y(GPa)$	$G_{xy}(GPa)$	ν_{xy}	$\alpha_1(^oC^{-1})$	$\alpha_2(^oC^{-1})$ [35]
124	8.4	4.7	0.3	$-4.5\cdot10^{-9}$	$5.2\cdot10^{-5}$

Table 1 Mechanical and thermal properties of the unidirectional ply

Two kinds of sixteen-layered multidirectional laminates were produced with a Teflon film embedded at mid-thickness during the piling up process in order to make the initial crack.

Five specimens of each sequence were cut with a diamond disc saw, being the nominal thickness and width of the specimens 3 mm and 15 mm, respectively. The edges of the laminate were discarded for the preparation of the specimens. Piano hinges were bonded to the specimens and tests were performed using a universal testing machine MTS–Insight 10 with a load cell of 250 N as shown in Fig. 5. In order to avoid the influence of the resin rich area the specimens were precracked in mode II, by a 3-point bending test. After this process, the nominal crack length was 40mm approximately, which makes the specimens suitable for application of beam theory [2].

Prior to DCB tests, the longitudinal flexural modulus was measured for every specimen by means of three-point bending tests at different spans, obtaining similar values for both configurations [36]. The resulting average value was 14.2 GPa .

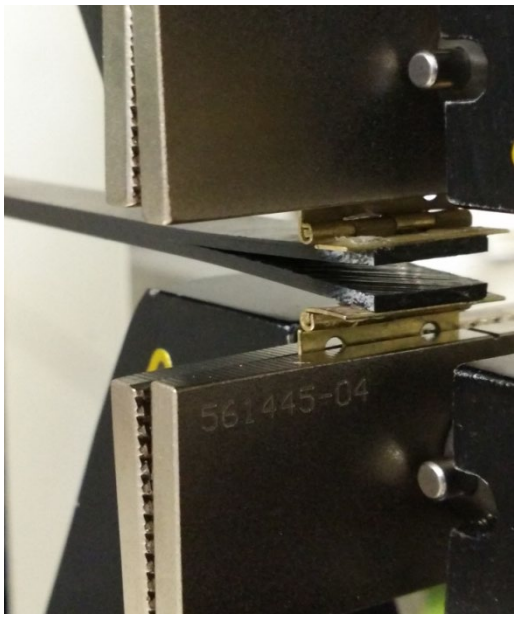

Fig. 5 DCB test configuration.

5. Results

5.1. Load-displacement curves

Load-displacement curves of both sequences studied are shown in the Fig. 6. As can be observed, the critical point corresponding to crack initiation is not easy to define. As a consequence, standards [1, 2] propose three points on the load-displacement curve to determine the crack onset value for unidirectional specimens, these are, the deviation from linearity point (NL), the 5% compliance increase (5% offset) and the one observed visually (VIS). In the case of multidirectional specimens, due to its lack of straight crack front, the latter is not meaningful. The NL point is sometimes ambiguous since nonlinear behavior may be due to other reasons such as local crack growth while the 5% offset point is a less scattered method than NL, but it produces higher values [37]. The non linear point has been used for calculations presented in this study.

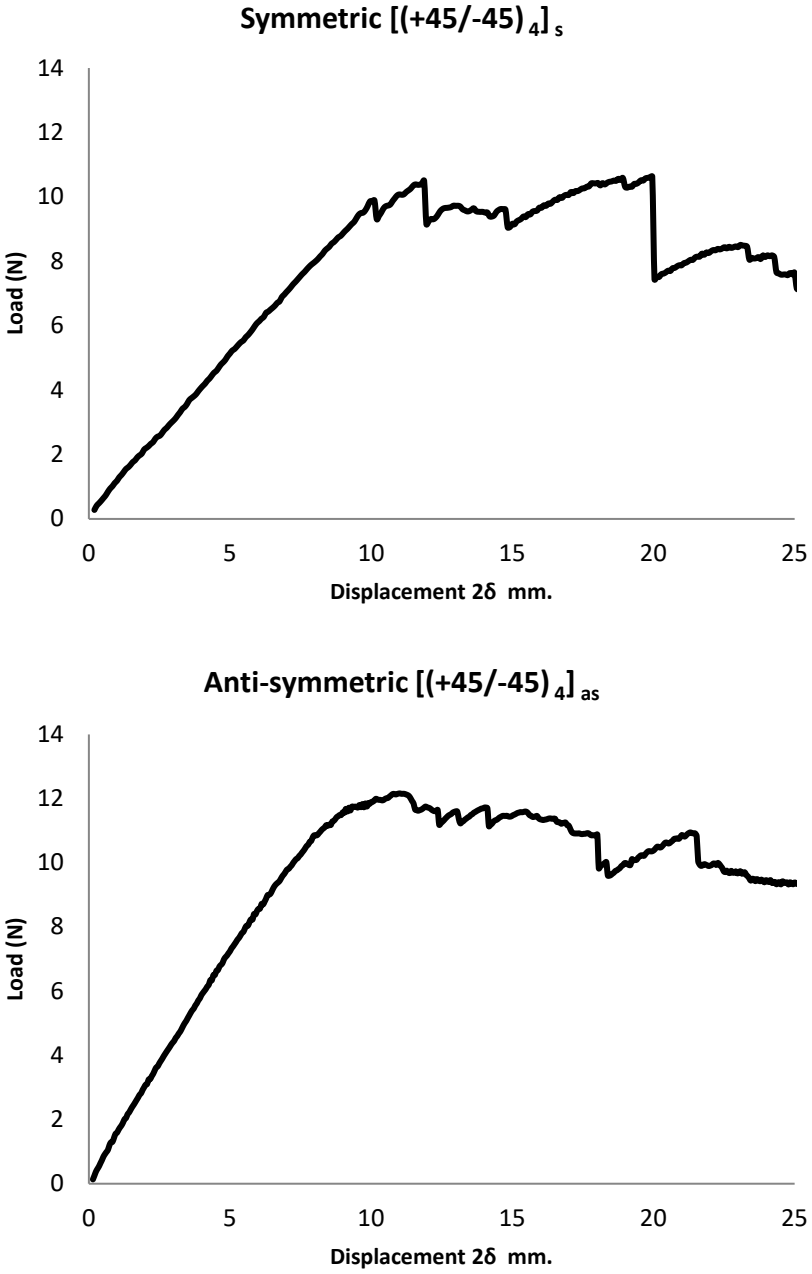

Fig. 6. Load-displacement curves.

5.2. Crack propagation

As it was expected, a pronounced thumbnail shaped crack front is observed during delamination. This is the effect of the curvature in the *y* axis which provokes a maximum strain in the middle of the crack front [11].

Two different crack propagation modes have been observed during the tests. On the one

hand, every anti-symmetric specimen showed similar shape of crack propagation. Crack starts propagating through one of the adjacent plies, however, immediately after propagation starts, on one side of the specimen the crack crosses this adjacent ply and propagates through the next one (Fig. 7). This latter crack expands linearly taking up the complete crack front after an advance equal to the specimen´s width. Thereafter, since the specimen has two arms with different thickness, crack continues its advance a few millimeters before the described process starts again increasing the difference between the thicknesses of the arms. This manner of crack propagation has been described by Laksimi et al. [13].

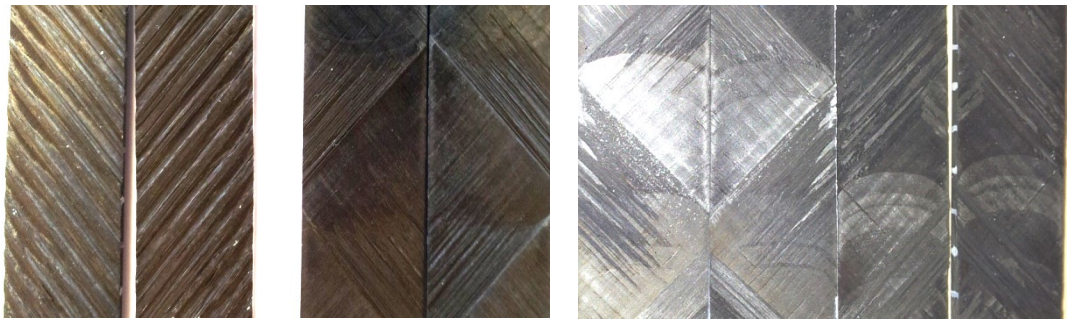

(a) $[\pm 45^{o}]_{4s}$ (b) $\left[(\pm 45^{o})_{4}\right]_{as}$

Fig. 7. Crack propagation surfaces. a) Symmetric specimen; b) Anti-Symmetric specimen.

On the other hand, while three of the symmetric specimens showed the same behavior as the anti-symmetric ones, a different crack propagation process was observed in the others. In this case, the crack propagated in a zig-zag fashion. As can be observed in Fig. 7, the crack advanced simultaneously in the mid-layer and in the adjacent ply. A similar geometrical structure has been reported before for cross-ply specimens [38].

The behaviors described provoke an asymmetry between the specimen arms. Consequently, the specimen has a rotation similar to that in ADCB tests related to mode II, as it is shown in Fig. 8. That complex combination of modes could be analyzed by

modeling the problem with 3D Finite Element Method and the Virtual Crack Closure Technique (VCCT).

In view of the above, the use of a visually measured crack length values beyond the end of the pre-crack are questionable. In the present paper, values of crack length used to calculate G have been obtained through the method presented in [29]. This method leads to calculate an effective crack length for every pair of load and displacement values based on the change of the compliance. Moreover, as hygrothermal effects are constant, the slope of the load-displacement curve does not change with respect to that reference and the same method can be used.

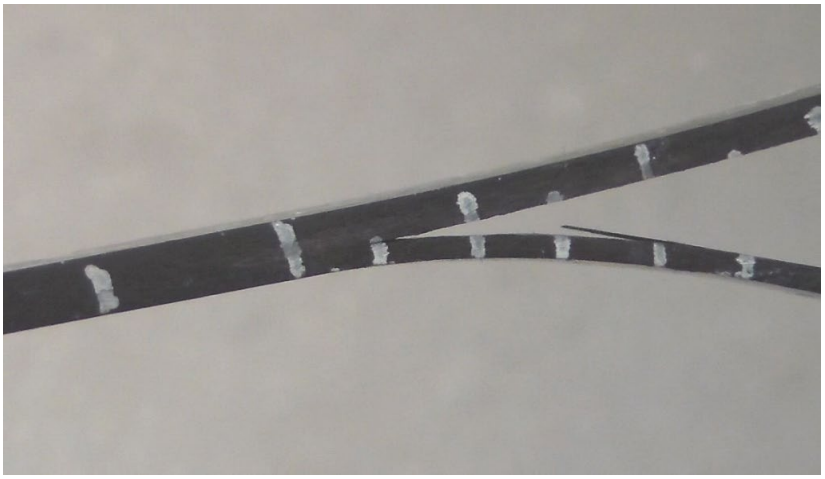

Fig. 8 Rotation of the specimen due to the asymmetry of the cracked arms.

5.3. Critical Energy Release Rate

Taking into account the propagation behavior observed and according to other authors [6] only initiation values will be considered to calculate interlaminar properties. In order to compare the results obtained by means of the proposed model, G will also be calculated through the modified beam theory (MBT) with crack length correction proposed by Williams [17] and by means of the "area" method. According to Shokrieh [39], the method developed by Williams leads to reliable results in angle-ply DCB

specimens. It has been used by several authors for calculating G_I in multidirectional laminates [13, 40, 41]. Unlike this method, other models habitually used to calculate G_{Ic} such as the Corrected Beam Theory, the Berry´s Compliance Calibration Method and the Modified Compliance Calibration Method will not be considered in this paper because they require propagation values and as stated above these values are not reliable.

Regarding the area method, it is worth noting that values obtained by this method can not readily be associated with any particular crack length, because it involves an average value between two increments of crack length [42]. Nevertheless, as the crack length has been determined for every pair of load-displacement values, a minimum crack growth of 1mm has been considered for calculations. Therefore, further propagation values are not considered and the average calculated values can be related to a determinate initial crack length.

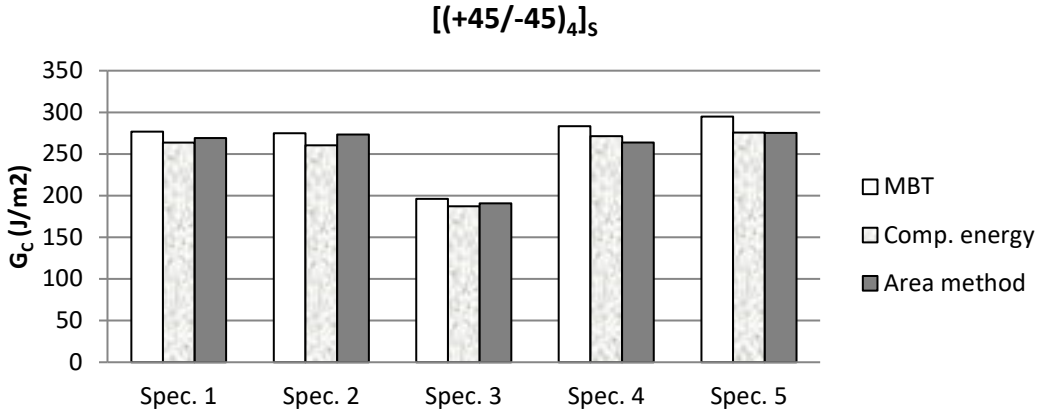

Fig. 9 Critical energy release rate for five symmetric specimens.

Fig. 9 shows G_c obtained through the three methods described for five symmetric specimens. Results calculated through the MBT are, in general, slightly higher than the others. It may be due to the fact that this method does not take into account hygrothermal effects that, as has been calculated in section 3.1.2, lead to a negative

term. The value of this term, and so, the part of mode III energy release rate for the studied symmetric specimens is $G_{III} = -8,7 J/m^2$.

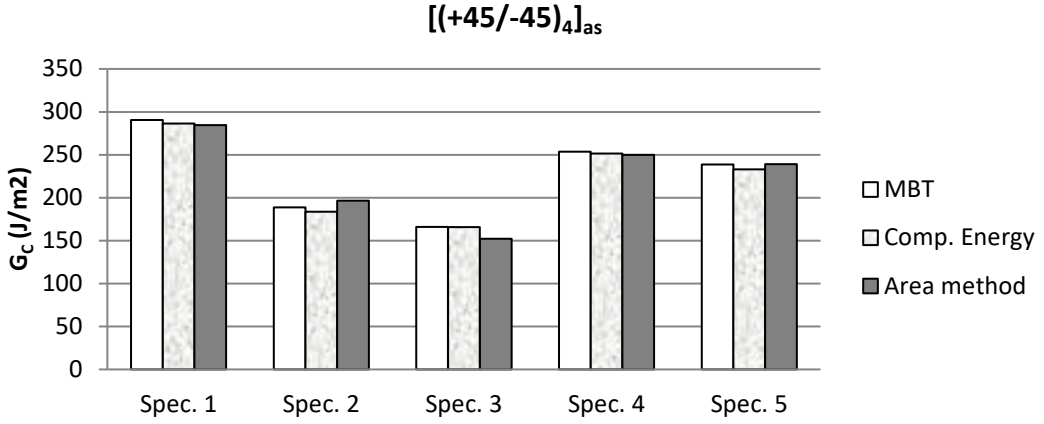

Fig. 10 Critical energy release rate for five anti-symmetric specimens.

In the case of anti-symmetric laminates, Fig. 10, results for different specimens also vary quite a lot. However, values obtained for each specimen through different methods are very similar. For this configuration, the negative term that includes hygrothermal effects (Section 3.1.3) results in $G_{III} = -9,2 \cdot 10^{-3} J/m^2$, that is negligible. Fig. 11 shows the average values for G_C calculated for both configurations studied.

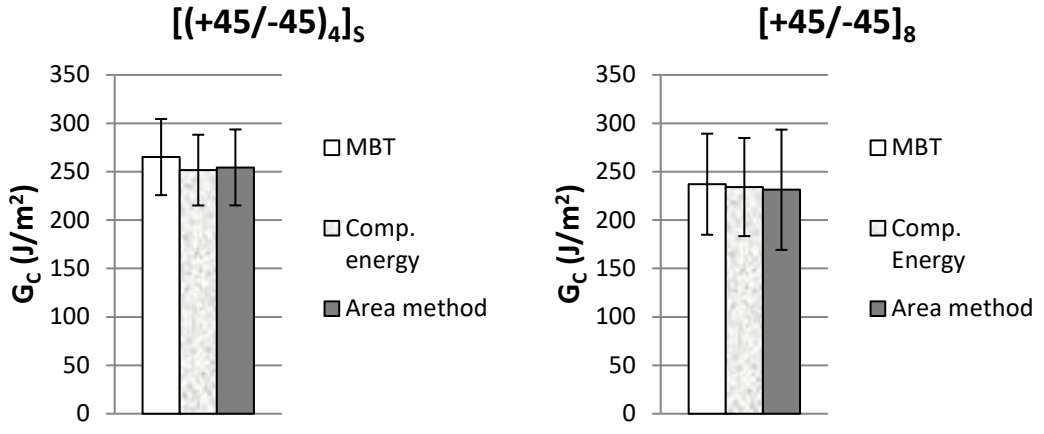

Fig. 11 Average critical Strain Energy Release Rate. a) Symmetric laminate. b) Anti-symmetric laminate.

6. Summary and conclusions

An analytical and experimental study regarding the critical energy release rate in symmetric and anti-symmetric DCB specimens has been presented. It is an extension of a previous model for unidirectional laminates. Laminates with anti-symmetric cracked arms have been analyzed.

An expression for the energy release rate has been obtained for both cases, symmetric and anti-symmetric laminates including hygrothermal effects. In both cases, these effects lead to a negative contribution to the energy release rate associated with mode III fracture.

Two crack propagation modes have been observed, leading both of them to an advance through different plies. The consequent asymmetry between the cracked arms provokes a rotation related to mode II. Therefore, only initial crack advance values have been taken into account that propagation values are not reliable.

The consideration of the hygrothermal effects in the material studied results in a decrease of an approximate 3% of the energy release rate for symmetric laminates, while the effect on those anti-symmetric is below 1%.

References

[1] ISO, « 15024, Fiber-reinforced Plastic Composites – Determination of Mode I Interlaminar Fracture Toughness, GIc, for Unidirectionally Reinforced Materials,» (2001.

[2] ASTM, «Standard D5528-94a, Standard Test Method for Mode I Interlaminar Fracture Toughness of Unidirectional Continuous Fiber Reinforced Polymer Matrix Composites,» Philadelphia, 1994.

[3] M. M. Shokrieh, A. Zeinedini, «A novel method for calculation of strain energy release rate of asymmetric double cantilever laminated composite beams,» *Applied Composite Materials,* vol. 21, pp. 399-415, 2014.

[4] M. J. Hiley, «Delamination between multi-directional ply interfaces in carbon-epoxy composites under static and fatigue loading,» *European Structural Integrity Society,* vol. 27, pp. 61-72, 2000.

[5] A. B. de Morais, M. F. de Moura, A. T. Marques, P. T. de Castro, «Mode-I interlaminar fracture of carbon/epoxy cross-ply composites,» *Composites Science and Technology,* vol. 62, p. 679–686, 2002.

[6] A. B. Pereira, A. B. de Morais, «Mode I interlaminar fracture of carbon/epoxy multidirectional laminates,» *Composites Science & Technology,* vol. 64, pp. 2261-2270, 2004.

[7] M. M. Shokrieh, M. Heidari-Rarani, M. R. Ayatollahi, «Calculation of GI for a multidirectional composite double cantilever beam on two-parametric elastic foundation,» *Areospace Science and Technology,* vol. 15, pp. 534-543, 2011.

[8] D. Nicholls, J. Gallaguer, «Determination of GIC in Angle Ply Composites Using a Cantilever Beam Test Method,» *Journal of Reinforced Plastics and Composites,* vol. 2, pp. 2-17, 1983.

[9] B. D. Davidson, R. A. Schapery, «Effect of finite width on deflection and energy release rate of an orthotropic,» *Journal of Composite Materials,* vol. 22, pp. 640-656, 1988.

[10] B. Davidson, «An Analytical Investigation of Delamination Front Curvature in Double Cantilever Beam Specimens,» *Journal of Composite Materials,* vol. 24, pp. 1124-1137, 1990.

[11] B. Davidson, R. Krüger, M. König, «Effect of stacking sequence on energy release rate distributions in multidirectional dcb and enf specimens,» *Engineering Fracture Mechanics,* vol. 55, nº 4, pp. 557-569, 1996.

[12] A. B. de Morais, «Double cantilever beam testing of multidirectional laminates,» *Composites: Part A,* vol. 34, nº 12, pp. 1135-1142, 2003.

[13] A. Laksimi, A. Ahmed Benyahia, M. L. Benzeggagh, X. L. Gong, «Initiation and bifurcation mechanisms of cracks in multi-directional laminates,» *Composites Science and Technology,* vol. 60, pp. 597-604, 2000.

[14] P. Robinson, D. Q. Song, «Robinson, Song. A Modified DCB Specimen for Mode I Testing of Multidirectional Laminates,» *Journal of Composite Materials,* vol. 26, nº 11, pp. 1554-1577, 1992.

[15] N. S. Choi, A. J. Kinloch, J. G. Williams, «Delamination Fracture of Multidirectional Carbon-Fiber/Epoxy Composites under Mode I, Mode II and Mixed Mode I/II Loading,» *Journal of Composite Materials,* vol. 33, nº 1, pp. 73-100, 1999.

[16] M. F. Kanninen, «An augmented double cantilever beam model for studying crack propagation and arrest,» *International Journal of Fracture,* vol. 9, nº 1, p. 83.92, 1971.

[17] J. G. Williams, «End corrections for orthotropic DCB specimens,» *Compos Sci Technol,* vol. 35, nº 4, pp. 367-376, 1989.

[18] F. Ozdil, L. Carlsson, «Beam analysis of angle-ply laminate DCB specimens,» *Composites Science and Technology,* vol. 59, pp. 305-315, 1999.

[19] R. Olsson, «A simplified improved beam analysis of the DCB specimen,» *Compos Sci Technol,* vol. 43, p. 329–338, 1992.

[20] A. Szekrényes, «Improved analysis of unidirectional composite delamination specimens,» *Mechanics of Materials,* vol. 39, pp. 953-974, 2007.

[21] M. M. Shokrieh, M. Heidari-Rarani, M. R. Ayatollahi, «Interlaminar fracture toughness of unidirectional DCB specimens: A novel theoretical approach,» *Polymer Testing,* vol. 31, p. 68–75, 2012.

[22] J. R. Weatherby, *Evaluation of energy release rates in unidirectional double cantilevered beam fracture specimens,* MSc Thesis: Texas A&M University, 1982.

[23] R. Nageswara, R. Acharya, «Evaluation of fracture energy GIC using a double cantilever beam fibre composite specimen,» *Engineering Fracture Mechanics,* vol. 51, nº 2, pp. 317-322, 1995.

[24] V. A. Franklin, T. Christopher, «Fracture Energy Estimation of DCB Specimens Made of GlassEpoxy, An Experimental Study,» *Advances in Materials Science and Engineering,* vol. 2013, p. 7, 2013.

[25] A. B. de Morais, «Mode I cohesive zone model for delamination in composite beams,» *Engineering Fracture mechanics,* vol. 109, pp. 236-245, 2013.

[26] M. M. Shokrieh, M. Heidari-Rarani, S. Rahimi, «Influence of curved delamination front on toughness of multidirectional DCB specimens,» *Composite structures,* vol. 94, pp. 1359-1365, 2012.

[27] T. A. Sebaey, N. Blanco, C. S. Lopes, J. Costa, «Numerical investigation to prevent crack jumping in Double Cantilever Beam tests of multidirectional composite laminates,» *Composites Science and Technology,* vol. 71, pp. 1587-1592, 2011.

[28] J. A. Nairn, «Energy release rate analysis for adhesive and laminate double cantilever beam specimens emphasizing the effect of residual stresses,» *International Journal of Adhesion & Adhesives,* vol. 20, pp. 59-70, 2000.

[29] J. De Gracia, A. Boyano, A. Arrese, F. Mujika, «A new approach for determining the R-curve in DCB tests without optical measurements,» *Engineering Fracture Mechanics,* vol. 135, pp. 274-285,

2015.

[30] I. Daniel, O. Ishai, Engineering mechanics of composite materials, New York: Oxford university press , 2006.

[31] F. Mujika, «A novel approach for the three point flexure test of multidirectional laminates,» *Journal of Composite Materials,* vol. 46, nº 3, pp. 259-274, 2011.

[32] A. Boyano, J. de Gracia, A. Arrese, F. Mujika, «Equivalent energy release rate and crack stability in the End Notched Flexure with inserted roller mixed mode I/II test,» *Theoretical and Applied Fracture Mechanics,* vol. 87, pp. 99-109, 2017.

[33] V. Vasiliev, E. Morozov, Advanced mechanics of composite materials, Elsevier Science and Technology, 2007.

[34] J. Romera, M. Cantera, I. Adarraga, F. Mujika, «A top-down analytic approach for the analysis of edge effects of angle-ply symmetric laminates,» *Composite Structures,* vol. 104, pp. 60-70, 2013.

[35] M. Cantera, J. Romera, I. Adarraga, F. Mujika, «Hygrothermal effects in composites:Influence of geometry and determination of transverse coefficient of thermal expansion,» *Journal of Reinforced Plastics and co mposites,* vol. 31, nº 19, pp. 1270-1281, 2012.

[36] F. Mujika, «On the effect of shear and local deformation in three-point bending tests,» *Polym Test,* vol. 26, pp. 869-877, 2007.

[37] X. J. Gong, A. Hurez, G. Verchery, «On the determination of delamination toughness by using multidirectional DCB specimens,» *Polymer Testing,* vol. 29, pp. 658-666, 2010.

[38] A. B. de Morais, M. F. de Moura, A. T. Marques, P. T. de Castro, «Mode-I interlaminar fracture of carbon/epoxy cross-ply composites,» *Composites Science and Technology,* vol. 62, pp. 679-686, 2002.

[39] M. M. Shokrieh, M. Heidari-Rarani, «A comparative study for beams on elastic foundation models to analysis of mode-I delaminations in DCB specimens,» *Structural Engineering and Mechanics,* vol. 37, nº 2, pp. 149-162, 2011.

[40] A. de Morais, «A new fibre bridging based analysis of the Double Cantilever Beam (DCB) test,» *Composites: Part A,* vol. 42, p. 1361–1368, 2011.

[41] P. Qiao, F. Chen, «On the Compliance and Energy Release Rate of Generically-unified Beam-type Fracture Specimens,» *Journal of Composite Materials,* vol. 45, pp. 65-101, 2011.

[42] S. Hashemi, A. J. Kinloch, J. G. Williams, «Corrections needed in double-cantilever beam tests for assessing the interlaminar failure of fibre-composites,» *Journal of Materials Science Letters,* vol. 8, pp. 125-129, 1989.